pISSN 1976-913X
eISSN 2092-805X

J Inf Process Syst, Vol.9, No.1, March 2013 http://dx.doi.org/10.3745/JIPS.2013.9.1.103

# A TRUS Prostate Segmentation using Gabor Texture Features and Snake-like Contour

Sung Gyun Kim* and Yeong Geon Seo**

**Abstract**—Prostate cancer is one of the most frequent cancers in men and is a major cause of mortality in the most of countries. In many diagnostic and treatment procedures for prostate disease accurate detection of prostate boundaries in transrectal ultrasound(TRUS) images is required. This is a challenging and difficult task due to weak prostate boundaries, speckle noise and the short range of gray levels. In this paper a method for automatic prostate segmentation in TRUS images using Gabor feature extraction and snake-like contour is presented. This method involves preprocessing, extracting Gabor feature, training, and prostate segmentation. The speckle reduction for preprocessing step has been achieved by using stick filter and top-hat transform has been implemented for smoothing the contour. A Gabor filter bank for extraction of rotation-invariant texture features has been implemented. A support vector machine(SVM) for training step has been used to get each feature of prostate and nonprostate. Finally, the boundary of prostate is extracted by the snake-like contour algorithm. A number of experiments are conducted to validate this method and results showed that this new algorithm extracted the prostate boundary with less than 10.2% of the accuracy which is relative to boundary provided manually by experts

**Keywords**—Gabor Filter Bank, Support Vector Machines, Prostate Segmentation

## 1. INTRODUCTION

Prostate cancer is the most frequently diagnosed cancer in men and the second cancer-related cause of death for them [1, 2]. According to the American Cancer Society, dead rate is decreasing every year caused by prostate cancer, but in 2007 23 out of every 100,000 people died of prostate cancer [3]. The rate is second highest value following the dead rate of lung and bronchial cancer. Hence diagnosis of the cancer of the early stages is crucial. Ultrasound imaging is a widely used technology for diagnosing and treatment this kind of cancer [4]. Especially, prostate transrectal ultrasound (TRUS) prostate images are captured easier and with lower cost. In fig. 1, an example of TRUS image capture is shown.

For the purpose of prostate cancer diagnosis and image-guided surgical planning and therapy, the segmentation of prostates from two-dimensional or three-dimensional ultrasound images is challenged. US imaging is the main modality for prostate cancer diagnosis and treatment. Accurate segmentation of prostate boundaries from US images plays an important role in many pros-

※ This work was studied by research fund for supporting the professor of GNU research year program in 2011
Manuscript received March 24, 2012; first revision August 16, 2012; accepted October 30, 2012.
**Corresponding Author: Yeong Geon Seo**
* Computer Institute, Gyeongsang National University, Jinju, Korea(buti2318@gmail.com)
** Dept. of Computer Science, Gyeongsang National University, Jinju, Korea(young@gnu.ac.kr)

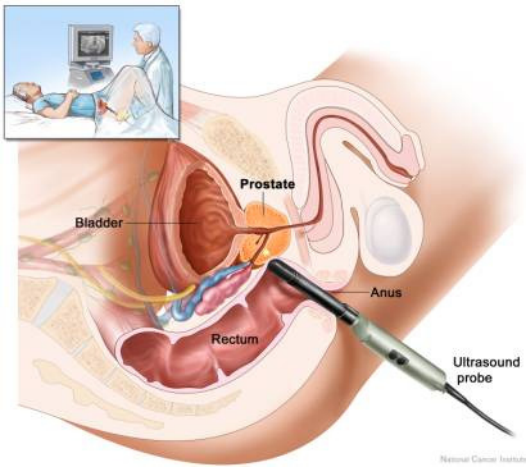


Fig. 1. Placements of human organs and US probe

tate-related applications such as the accurate placement of the needles and the biopsy, the assignment of the appropriate therapy in cancer treatment, and the measurement of the prostate gland volume [5]. Moreover, the shape of the prostate in US images is considered as an important indicator for staging prostate cancer. But, because the boundaries between prostate and nonprostate of the image are ambiguous, an automatic extraction of the boundaries has some difficulties [6, 7]. Such that, they are very weak texture structure, low contrast, fuzzy boundaries, speckle noise and shadow regions. To cope with these problems, different methods have been studied.

Zhan and Shen [6] developed a deformable segmentation using Gabor-support vector machine (G-SVM) based 3D prostate images. Pathak and etc [8] presented a new paradigm for the edge-guided delineation, providing the algorithm-detected prostate edges as a visual guidance for the user to manually edit. Shen and etc [9] designed a statistical shape model for outlining prostate boundary from 2D TRUS images. Shao and etc [10] presented a level set based method to detect prostate surface from 3D US images. Yan and etc [11] proposed an automatic segmentation for the prostate from 2D TRUS using adaptive learning local shape statistics. Akbari and etc [12] presented an automatic segmentation of the prostate in 3D TRUS images by extracting texture features and by statistically matching geometrical shape of the prostate. Until now, there have been so many studies, but most studies needed a help of human expert and who or what did not find any tumors.

Our studies consist of preprocessing, extracting Gabor feature, training and prostate segmentation. Preprocessing step processes histogram equalization, removing background, removing probe and stick filtering for removing speckle noise. The reason why it removes the background and the probe is to reduce the computing space. The removed spaces absolutely are nonprostate region. Histogram equalization enhances contrast and equalizes the contrasts of different images. Extracting Gabor feature step extracts and characterizes texture features in US images using Gabor filters at multiscales and multiorientations. Training step trains the Gabor texture features according to whether the pixels belong to prostate and nonprostate using SVM. By the results of SVM, each pixel of the test image is classified to prostate or nonprostate. And then, since none

of all pixels in the images are accurately classified, the final step applies snake-like algorithm and gets the smooth boundaries between them. The results experimented from our 20 test images made difference by 10.2% compared to the work done by human expert.

## 2. RELATED STUDIES

In this chapter, we present difficulties of US prostate segmentation, and then we present information on the Gabor transform, deformable segmentation and 3D segmentation which are very important in this paper.

### 2.1 Difficulties of US Prostate Segmentation

As shown in fig. 2, US prostate image has a lot of noise and is hard to delineate the boundaries. Especially, the base and apex parts of prostate are generally unclear or broken, since these boundaries are almost parallel to US beams of the transducer. Therefore, the images of the two parts are almost impossible to delineate the boundaries without reference of their neighbor's boundaries.

To cope with this problem, several methods were proposed. First, Chakraborty and etc [4] and Zhan and Shen [6] proposed a deformable segmentation method. The boundary of deformable model is subsequently driven to the boundary between the tentatively labeled prostate and nonprostate tissues, while its shape is limited by its pre-constrained shape. Tentative tissue labeling and subsequent deformation are repeated until they converge to the boundary in the prostate images. Another method is to use 3D segmentation [6, 12]. Using 3D image the method gets the statistical boundary model from the apex to the base. The boundaries of an image are adjusted within a certain limit of the pre-acquired 3D model. Disadvantages of these methods can't find abnormal protrusions like tumor.

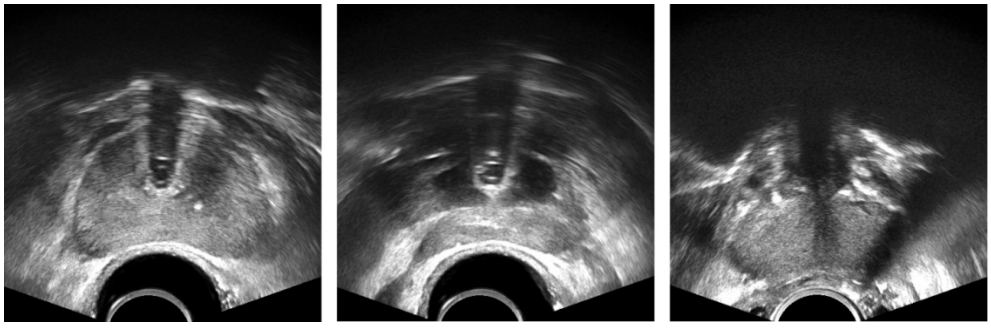

(a) (b) (c)

Fig. 2. (a) center image (b) base image (c) apex image

### 2.2 Gabor Transform

The Gabor transform, named after Dennis Gabor, is a special case of the short-time Fourier transform. It is used to determine the sinusoidal frequency and phase content of local sections of

a signal as it changes over time. The function to be transformed is first multiplied by a Gaussian function, which can be regarded as a window, and the resulting function is then transformed with a Fourier transform to derive the time-frequency analysis. The window function means that the signal near the time being analyzed will have higher weight. The Gabor transform of a signal *x(t)* is defined by this formula

$$G_x(t,f) = \int_{-\infty}^{\infty} e^{-\pi(\tau-t)^2} e^{-j2\pi f\tau} x(\tau) d\tau$$

The Gaussian function has infinite range and it is impractical for implementation. But take a look at the distribution of Gaussian function.

$$\begin{cases} e^{-\pi a^2} \geq 0.00001; & |\alpha| \leq 1.9143 \\ e^{-\pi a^2} < 0.00001; & |\alpha| > 1.9143 \end{cases}$$

Gaussian function with $|\alpha| > 1.9143$ can be regarded as 0 and also can be ignored. Here, $\alpha$ is time(sec). Thus the Gabor transform can be simplified as

$$G_x(t,f) = \int_{-1.9143}^{1.9143} e^{-\pi(\tau-t)^2} e^{-j2\pi f\tau} x(\tau) d\tau$$

This simplification makes the Gabor transform practical and realizable. Here, τ is window time at the center of window. The Gabor transform is invertible. The original signal can be recovered by the following equation.

$$x(t) = \int_{-\infty}^{\infty} G_x(t,f) e^{j2\pi tf} df$$

## 2.3 SVM

The standard SVM takes a set of input data and predicts, for each given input, which of two possible classes comprises the input, making the SVM a non-probabilistic binary linear classifier. Given a set of training examples, each marked as belonging to one of two categories, an SVM training algorithm builds a model that assigns new examples into one category or the other. The original optimal hyperplane algorithm proposed by Vapnik in 1963 was a linear classifier. Linear SVM gives some training data *D*, a set of *n* points of the form.

$$D = \{(x_i, y_i) \mid x_i \in R^p,\ y_i \in \{-1, 1\}\}_{i=1}^{n}$$

where the $y_i$ is either 1 or −1, indicating the class to which the point $x_i$ belongs. Each $x_i$ is a *p*-dimensional real vector. We want to find the maximum-margin hyperplane that divides the point shaving $y_i = 1$ from those having $y_i = -1$.

In 1992, Bernhard Boser, Isabelle Guyon and Vapnik suggested a way to create nonlinear classifiers by applying the kernel trick to maximum-margin hyperplanes [13]. The resulting algorithm is formally similar, except that every dot product is replaced by a nonlinear kernel func-

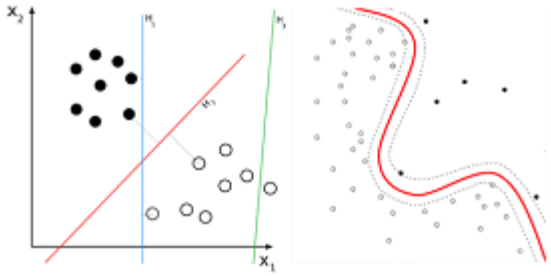

Fig. 3. An example of a linear SVM and a nonlinear SVM

tion. This allows the algorithm to fit the maximum-margin hyperplane in a transformed feature space. The transformation may be nonlinear and the transformed space high dimensional; thus though the classifier is a hyperplane in the high-dimensional feature space, it may be nonlinear in the original input space. Fig.3 shows an example of linear and nonlinear SVM, respectively.

### 2.4 Deformable and 3D Segmentation

Zhan and Shen [6] used deformable surface model and divided the whole temporary boundaries to several areas, named by subsurface. The model deforms under the influence of two basic components of an energy function. The two components are the internal and external forces as following equation.

$$E = Eext + \alpha Eint$$

The external energy *Eext* derives the mesh towards the surface patches obtained in the surface detection step. The internal energy *Eint* restricts the flexibility of the mesh. The parameter α weights the relative influence of each term. There are two types of deformable models described in the literature on parametric deformable models and level set-based deformable models [14]. Parametric models have been used in edge detection, object recognition, shape modeling, and motion tracking.

Ghanei and etc [15] designed a 3D discrete model to outline the prostate boundaries. The users are required to outline image to give an initialization model. This model is simply deformed under both the internal force such as the curvature of the surface, and both the external force such as the edge map. Akbari and etc [12] presented a method for automatic segmentation of the prostate by extracting texture features and by statistically matching geometrical shape of the prostate.

## 3. ROTATION-INVARIANT TEXTURE FEATURES AND SNAKE-LIKE CONTOUR BASED SEGMENTATION

In this chapter, we present overall structure of the proposed approach and the detail procedures. The overall structure consists of preprocessing, Gabor feature extraction, training and application steps as shown in fig. 4. In the figure, preprocessing, Gabor texture feature extraction and training steps are repeated several times as the training images.

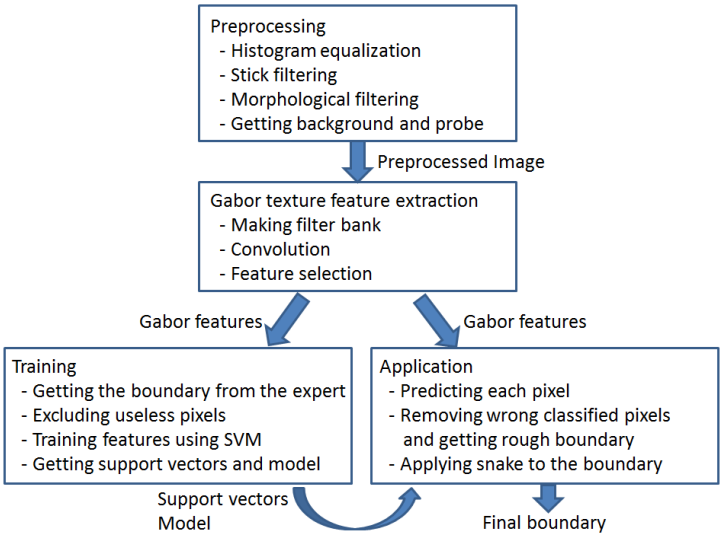


Fig. 4. Overall structure of the proposed method

### 3.1 Preprocessing

In preprocessing step, histogram equalization enhances the contrast of images by transforming the values in an intensity image, so that the histogram of the output approximately matches a specified histogram. Stick filtering filters to reduce the speckle noise. Morphological filtering is used to smooth filtered image and enhanced contrast near edges. Final step gets background and probe which will be excluded for training.

Histogram equalization considers a discrete gray scale image, x, and lets $n_i$ be the number of occurrences of gray level, $i$. The probability of an occurrence of a pixel level, $i$ in the image is

$$p_x(i) = p(x = i) = \frac{n_i}{n}, 0 \leq i < L$$

Here, $L$ is the total number of gray levels in the image, $n$ is the total number of pixels in the image, and $p_x(i)$ is in fact the image's histogram for pixel value $i$. The stick filtering algorithm challenges the problem of filtering speckle in US images without losing edge detail. The stick filter determines the mean of neighboring pixels in the direction of the stick - the most likely direction of the linear feature passing through (x, y). If $n$ is the stick's length, there are $2*n$-2 possible orientations. We use 5 length pixels as shown fig. 5.

In morphological filtering, the top-hat and bottom transformation are applied on output of stick filter ($Fs$) with using a ordinary neighborhood window. We use a disk with radius 3 in top-hat, bottom-hat transformation.

$$H_t = top - hat(F_s)$$

$$H_b = bot - hat(F_s)$$

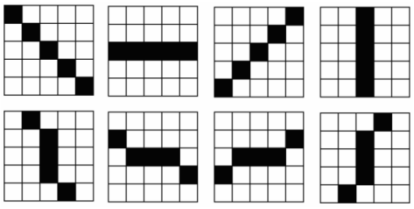

Fig. 5. A typical stick of five length pixels

$$F_p = F_s + H_t - H_b$$

$H_t$ is the top-hat and $H_b$ is the bottom-hat transformation and $F_p$ is the preprocessed image. We get background and probe, and then exclude them in step of training. Generally the background is black and is apparently unusable region. The probe which is generally an exploring needle in fig. 1 but is a half circle shaped black region in fig. 2. This is useless region as well.

### 3.2 Extracting Gabor Texture Features

Gabor filter bank is obtained by the dilation and rotation of the mother function. Here, we use that total numbers of the orientations are $K=4$, the scale numbers of the scales are $S = 2$. So the basic rotation and scale factors are $\psi=\pi/K$ and $a=(U_h/U_l)^{1/S-1}$ , respectively. $U_h$ and $U_l$ are parameters that determine the frequency range of the Gabor filter bank. We use $U_h =0.1$ and $U_l =0.025$. Using the scale variables and the rotation variables, the (s,k)th Gabor filter is

$$g_{s,k}(x,y) = a^s g(a^s(x\cos(k\psi)+y\sin(k\psi))\ a^s(-x\sin(k\psi)+y\cos(k\psi)))$$

The Gabor filter bank has two important properties, the frequency spectrum of the filter bank has a multiscale and multiorientation structure and each filter can be separated into two parts, i.e., the real part and the imaginary part. The real part is regarded as a smooth filter and the imaginary part is regarded as an edge detection filter. Using Gabor filter bank offers three advantages. First, it can smooth the image and remove speckle noises. Second, the multiscale structure enables hierarchical implementation. Third, the multiorientation structure enables the extraction of edge direction, edge strength and rotation-invariant features. We use the imaginary parts, but the real part Gabor features can be used. So the proper negotiation is needed. In this paper, we use 8 Gabor texture features per pixel which consist of $K$=4, $S$=2 and the imaginary part Gabor features.

### 3.3 Training the Features

To train the features using SVM, each pixel should be classified to prostate or nonprostate. Originally, no one knows whether each pixel belongs to which region. To classify the region, the human expert is needed. The inner part of the contours drawn by the expert is prostate and the outside of the contours is nonprostate. The pixels around the contour acquired from the expert and the useless region are excluded in the training process. Why the pixels around the contour are excluded is that they don't have classifiable features comparing to other regions.

Next, each pixel has 8 Gabor texture features which will be trained and have the following in-

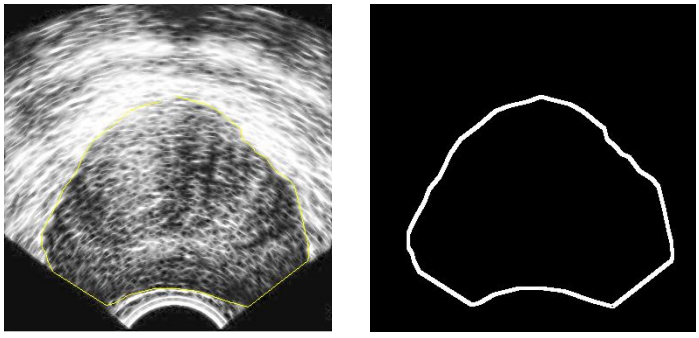

Fig. 6. Contour extracted from human expert and its neighbors which is not used for training

Table 1. Support vectors got from training

| Indices | Gabor texture features |
|---|---|
| (1,1) | 10.3537 |
| (1,2) | 11.3592 |
| (1,3) | 15.5525 |
| (1,4) | 16.1532 |
| (1,5) | 16.2178 |
| (1,6) | 15.9830 |
| (1,7) | 12.4169 |
| (1,8) | 11.4315 |

put format.

-1 1:33.248316 2:34.518724 3:19.255745 4:4.296715 5:33.996764 6:35.103513 7:19.049476 8:3.813344
1 1:-5.961116 2:-1.852036 3:2.131680 4:4.366701 5:-6.335777 6:-1.963415 7:1.260157 8:3.865562

First columns, -1 and 1 mean nonprostate and prostate, respectively. The numbers from 1 to 8 mean each pixel's Gabor feature orders that the first 4 features (1-4) are S=1 and K=1, 2, 3, and 4, and the next 4 ones (5-8) are S=2 and K=1, 2, 3, and 4, in the order named. The real numbers are the values of Gabor texture feature. After training the features, a number of support vectors and their coefficients are acquired. Table 1 is support vectors.

All the first values, 1s, are just indices that the values are from 1 to the number of support vectors, the second values, 1-8, are the same as the input indices. Their coefficients consist of -1 or 1 as the number of support vectors.

### 3.4 Classifying Pixels

In application step, a test image follows the preprocessing and Gabor transformation as training procedure, too. The input format for predicting whether each pixel belongs to prostate or nonprostate is same as one of training step. But here all the pixels are tested without excluding

any pixel. The results from prediction have -1 or 1, nonprostate or prostate, respectively. Fig. 7 shows a test image and its labels which the black ones are nonprostate, -1, and the white ones are prostate, 1.

First of all, wrong classified pixels are needed to be excluded from the labels. The algorithm to exclude the noise pixels is simple. The pixels not included in one big white label and the pixels not included in one big black label may be only excluded as shown in (a) of fig. 8. After removing noises, the contour has rough line around which the prostate and non prostate meet. Real prostate boundary doesn't have protrusion, so protrusions need to be removed. We use 7x7 mask as shown in fig. 9. This mask is used to find a block that one side is opened and the other sides are closed in different sides. The result after removing the protrusions is shown in (b) of fig. 8.

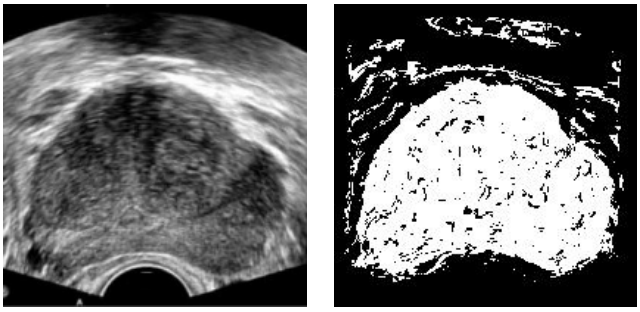

Fig. 7. A test image and its predicted labels

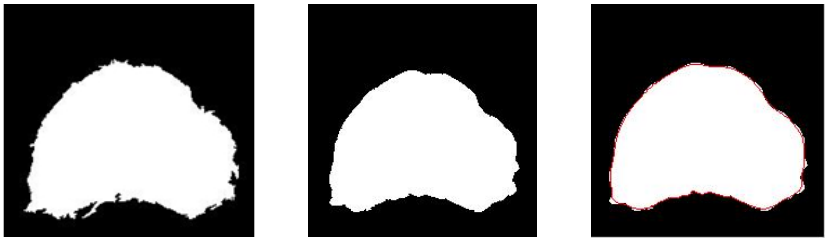

(a) (b) (c)

Fig. 8. (a) Labels after excluding wrong classified labels (b) Labels after removing protrusion (c) Labels after smoothing the contour with radius = 30

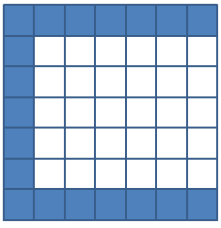

Fig. 9. Mask for removing the protrusion

### 3.5 Smoothing the Contours

A contour of a 2D region is defined by an ordered set of points where the neighboring elements contain the neighboring points. Such representation can be obtained with many techniques such as boundary tracing and chain codes. In a simple 2D point set or a curve the points do not have to line in a specific order. The contour smoothing is done by projecting all the contour points onto the local regression line. For each point, N neighboring points which lie on the contour are sampled on each side and a local regression line is computed. Then the current point is projected on this line. Applying this algorithm to all the points smoothes the contour and in a way brings the points closer. 2N+1 is the number of total points contributing to the computation of the local regression line. The higher the number of point is, the smoother the curve is.

Because of the linear nature of fitting, when too much smoothing is desired, some important features such as protrusions may be lost. In a way, this is an example of over-smoothing. A way to be less prone to such errors is to use Gaussian weighted least squares fit. To do this, the algorithm is the following and the labels after smoothing with radius = 30 shows in fig. 8 (c).

```
chain_code[1..2][]=Convert2DContours(x_pos, y_pos) ; // x_pos and y_pos are bin image
maxX = max(chain_code[1][]) ;
maxY = max(chain_code[2][]) ;
minX = min(chain_code[1][]) ;
minY = min(chain_code[2][]) ;
For all j of chain_code[1..2][j] with radius(=30 or 20)
   [xm, ym] = middle_point(chain_code[i][j], radius*2+1) ;
   [a, b, c] = weighted_ortho_least_square(xm, ym, chain_code[1..2][j]) ;
   [x2, y2] = project_point_on_line(a, b, c, chain_code[1..2][j]) ;
        if (x2>=minX && y2>minY && x2<=maxX && y2<=maxY)
Xs[j]=x2;
Ys[j]=y2;
else
Xs[j]=chain_code[1][j];
Ys[i]=chain_code[2][j];
end
   end // Final Xs and Ys are the smoothed contour
```

## 4. EXPERIMENTAL RESULTS

This chapter shows our experimental results in predicting pixels and the boundary between prostate and nonprostate. And we compare the boundaries of ours and expert in objective view and subjective view.

### 4.1 Predicting Pixels from SVM

We used SVM to predict whether each pixel is prostate or nonprostate using the training model. Fig. 10 shows testing images, their predicting labels, and labels after removing the island labels, which the white labels are predicted as prostate and the black labels as nonprostate. The

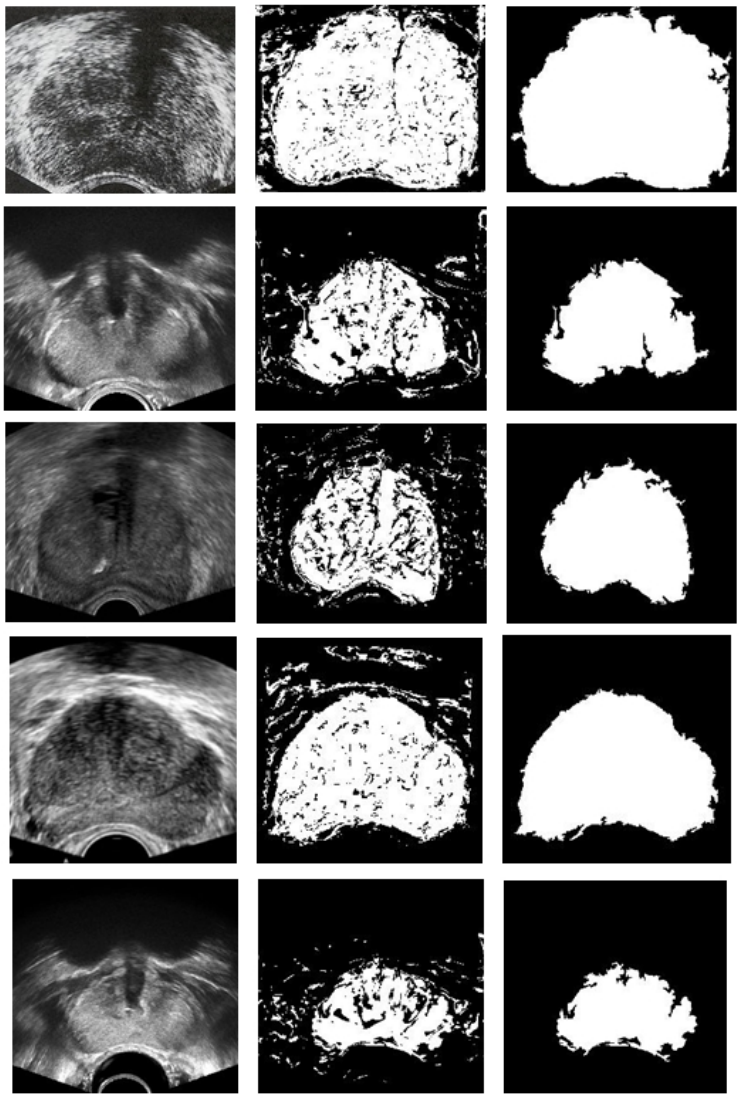

Fig. 10. Testing images, their predicting labels and labels after removing islands

reason the white labels are distributed in the black labels is why the texture features of them are similar, so removing the island labels is needed. Parameter used in Gabor filter bank that frequency is [0.025, 0.05, 0.1], orientation is [pi/4, pi/2, pi*3/4, pi], scale is [1, 2] and matrix size is 26, so center point of the matrix is [13, 13]. To remove protrusions we use 7x7 mask and to smooth the contour we use radius, 20 and 30.

## 4.2 Comparisons of Objective and Subjective Views

As shown in fig. 11, the boundaries by human expert and the proposed method are very similar but not same. Actually, even human experts have differences of their drawn boundaries. In

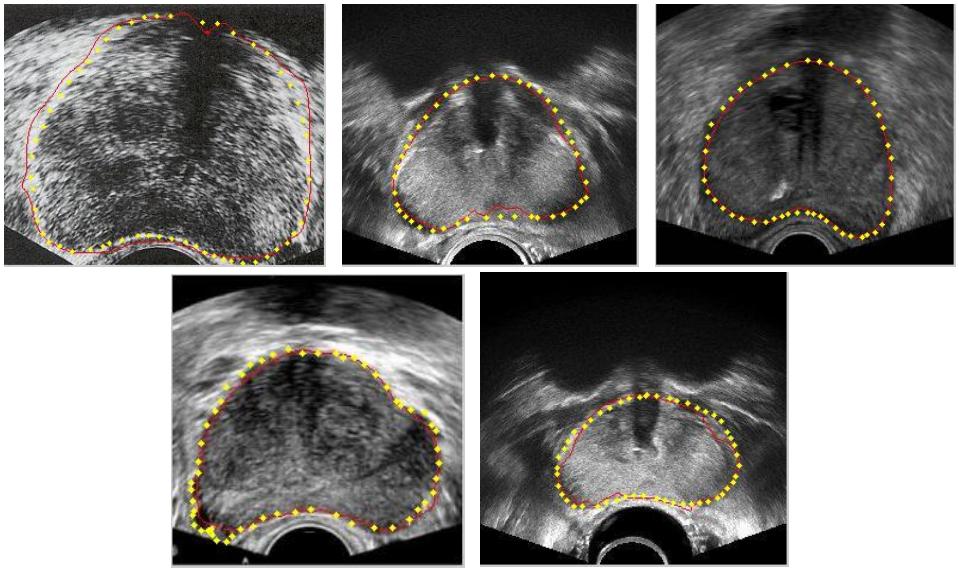

Fig. 11. Delineating boundaries by human expert (dotted line) and the proposed method (solid line)

the figure, the solid line is the delineating boundaries by the proposed method and the dashed line is one by experts. For quantitative comparison, we used difference between two boundaries. In this paper, we can use radius = 20 or 30, however, the figure shows radius = 30. The difference (D) comes from the following equation.

$$D = count(\text{for all pixels } E(x, y) \text{ and } P(x,y), \text{ labels}(E(x,y) \mathrel{!}= P(x,y))) \,/\, count(\text{prostate of } E),$$

Here, E means expert, P means the proposed method.

Table 2 shows *D* for 5 images of 20 testing images. Although the difference between the boundaries of human expert and the proposed method is bigger than other test images, *D* is not too big because the size of the prostate is occupying the big region. The value, 0.109, means that 10.9% labels are wrong classified. The wrong classified labels are distributed on the boundary of prostate and nonprostate. It took 5.2 seconds on average for 20 experimental images.

## 5. CONCLUSION

This paper proposed a TRUS prostate segmentation using Gabor texture features, SVM, and snake-like contour smoothing algorithm. As the boundary between prostate and nonprostate is not clear and even the textures of them are hard to classify, especially for US prostate image. First, after processing the training images, the pixels (1 or -1) that human expert classifies all the pixels as prostate and nonprostate region are transformed by Gabor filter bank. Gabor texture features acquired by the transform are trained by SVM whose outputs are support vectors. These support vectors are used for classifying the pixels with prostate and nonprostate. Finally the test image is classified with two regions which are not clear. Using noise reduction and protrusion

removal, a rough contour is determined and is smoothed by snake-like algorithm. The proposed method through these processing has difference about 10% comparing to human expert's contours. Our future studies is to improve the computation time, to apply human expert's knowledge, and finally to implement 3D segmentation.

## REFERENCES


[1] Cancer Facts and Figures. American Cancer Society. http://www.cancer.org

[2] Mettlin C: American society national cancer detection project. Cancer 1995, 75:1790-1794.

[3] http://www.cancer.org/Research/CancerFactsFigures/CancerFactsFigures/cancer-facts-figures-2011.

[4] A. Chakraborty, L. H. Staib, and J. S. Duncan, *"Deformable boundary finding in medical images by integrating gradient and region information," IEEE Trans. Med. Imag.*, Vol.15, No.6, December, 1996, pp.859-870.

[5] P. D. Grimm, J. C. Balsko, and H. Ragde, "*Ultrasound guided transperineal implantation of iodine 125 and palladium 103 for the treatment of early stage prostate cancer," Atlas Urol. Clin. No.Amer.*, Vol.2, 1994, pp.113-125.

[6] Y. Zhan and D. Shen **,** "*Deformable Segmentation of 3-D Ultrasound Prostate Images Using Statistical Texture Matching Method"***,** *IEEE Trans. on Medical Imaging*, Vol.25, March, 2006, pp.245-255.

[7] A. Rafiee, A. Salimi, and A. Roostam, *"A Novel Prostate Segmentation Algorithm in TRUS Images", World Academy of Science, Engineering and Technology 45*, 2008, pp.120-124.

[8] S. D. Pathak, V. Chalana, D. R. Haynor, and Y. Kim, *"Edge-guided boundary delineation in prostate ultrasound images", IEEE Trans. Med. Imag.*, Vol.19, No.12, December, 2000, pp.1211-1219.

[9] D. Shen, Y. Zhan, and C. Davatzikos, *"Segmentation prostate boundaries from ultrasound images using statistical shape model," IEEE Trans. Med. Imag.*, Vol.22, No.4, April, 2003, pp.539-551.

[10] F. Shao, K. V. Ling, and W. S. Ng, *"3-D prostate surface detection from ultrasound images based on level set method," in Proc. MICCAI 2003*, 2003, pp.389-396.

[11] P. Yan, S. Xu, B. Turkbey and J. Kruecker, "*Adaptively Learning Local Shape Statistics for Prostate Segmentation in US", IEEE Trans. On Biomedical Eng.*, Vol.58, No.3, March, 2011, pp.633-641.

[12] H. Akbari, X. Yang, L. Halig and B. Fei, *"3D segmentation of Prostate Ultrasound images Using Wavelet Transform", Proc. of SPIE* 7962, 2011.

[13] B. E. Boser, I. M. Guyon and V. N. Vapnik.*"A training algorithm for optimal margin classifiers", In D. Haussler, editor, 5th Annual ACM Workshop on COLT*, 1992, pp.144-152.

[14] J. Suri and A. Farag, *"Deformable Models 2", Springer*, 2007, pp.75-94.

[15] A. Ghanei, H. S. Zadeh, A. Ratkesicz, and F. Yin, *"A three-dimensional deformable model for segmentation of human prostate from ultrasound image," Med. Phys.,* Vol.28, 2001, pp.2147-2153.



**Sung Gyun Kim**

He received BS, MS and Ph.D. degrees in Computer Science from GNU in 1992, 2003 and 2008, respectively. During 1992 - 1995 and 2000 - current, he is working for GNU, Computer Institute. During 1996 - 2000, he worked for Seoul National Univ., Computer Institute. His research interests include medical imaging, information system for student and mobile web.

**Yeong Geon Seo**

He received a BS degree from Computational Statistics of Gyeongsang National Univ.(GNU) and, MS and Ph.D. degrees from Computer Science of Soongsil Univ. in 1987, 1989 and 1997, respectively. During 1989 - 1992, he worked in Trigem Computer Inc. to develop 4GL(XL/4). And now he is working for GNU, dept. of Computer Science since 1997. His research interests include medical imaging, JPEG2000, 3D modeling of human organs and computer network.